

EXTREME BLIND IMAGE RESTORATION VIA PROMPT-CONDITIONED INFORMATION BOTTLENECK

Hongeun Kim* Bryan Sangwoo Kim* Jong Chul Ye

KAIST AI

*: Equal contribution

{hongeun, bryanswkim, jong.ye}@kaist.ac.kr

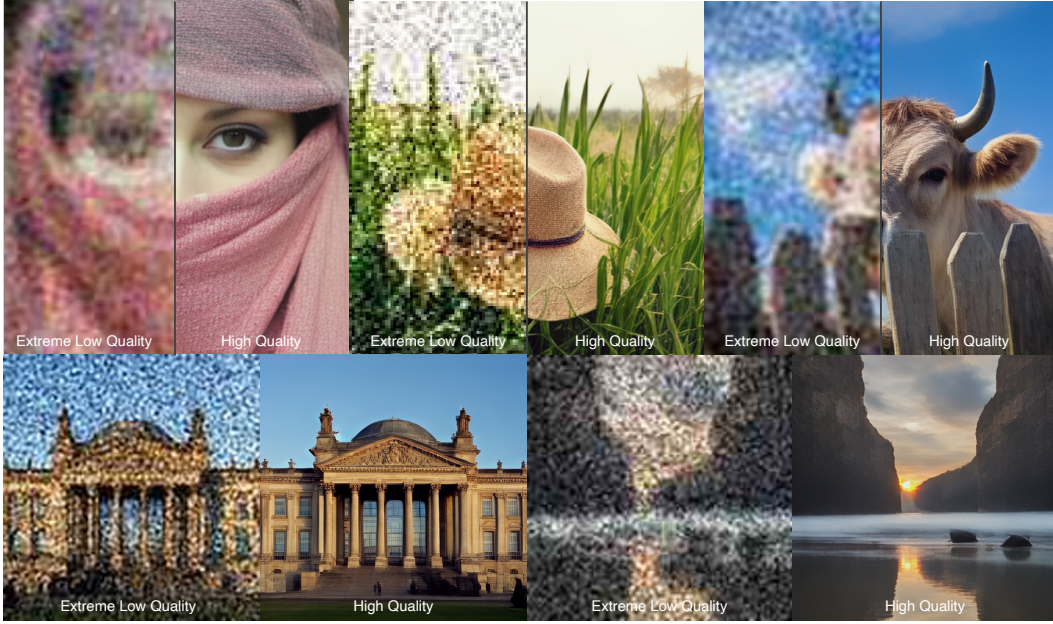


Figure 1: Extreme blind image restoration with our Prompt-Conditioned Information Bottleneck method for various fully blind images. Our method produces high-quality results with fine detail.

ABSTRACT

Blind Image Restoration (BIR) methods have achieved remarkable success but falter when faced with Extreme Blind Image Restoration (EBIR), where inputs suffer from severe, compounded degradations beyond their training scope. Directly learning a mapping from extremely low-quality (ELQ) to high-quality (HQ) images is challenging due to the massive domain gap, often leading to unnatural artifacts and loss of detail. To address this, we propose a novel framework that decomposes the intractable ELQ-to-HQ restoration process. We first learn a projector that maps an ELQ image onto an intermediate, less-degraded LQ manifold. This intermediate image is then restored to HQ using a frozen, off-the-shelf BIR model. Our approach is grounded in information theory; we provide a novel perspective of image restoration as an *Information Bottleneck* problem and derive a theoretically-driven objective to train our projector. This loss function effectively stabilizes training by balancing a low-quality reconstruction term with a high-quality prior-matching term. Our framework enables *Look Forward Once* (LFO) for inference-time prompt refinement, and supports plug-and-play strengthening of existing image restoration models without need for finetuning. Extensive experiments under severe degradation regimes provide a thorough analysis of the effectiveness of our work.

1 INTRODUCTION

Image restoration is a long-standing problem in computer vision that focuses on recovering a clean high-quality (HQ) image from its degraded low-quality (LQ) observation. Denoting the space of realistic HQ images as \mathcal{X}_{HQ} and the space of LQ images as \mathcal{X}_{LQ} , the objective is to learn the mapping,

$$\mathcal{R} : \mathcal{X}_{\text{LQ}} \rightarrow \mathcal{X}_{\text{HQ}} \quad (1)$$

In recent years, deep learning-based methods have achieved remarkable success in this domain, replacing traditional model-based approaches by learning powerful image priors directly from large-scale datasets (Zhang et al., 2017; Zamir et al., 2022; Wang et al., 2022; Liang et al., 2021; Dong et al., 2014; Chen et al., 2023). However, these methods often assume a simple, known degradation process, which is impractical for real-world scenarios where degradations are a complex combination of various factors (e.g., compression artifacts, sensor noise, motion blur, downsampling, etc). Such *blind* nature of real-world scenarios makes the already ill-posed problem of restoration significantly more difficult, as a single LQ image could theoretically result from numerous combinations of clean images and degradation functions (Wang et al., 2021; Zhang et al., 2021).

Blind Image Restoration (BIR) tackles this challenge directly by aiming to recover a high-quality, clean image from a low-quality counterpart without prior knowledge of the degradation. Recent methods in BIR (Chihaoui et al., 2024; Chihaoui & Favaro, 2025; Xiao et al., 2024; Lin et al., 2024) demonstrate impressive performance by modeling a rich and randomized space of synthetic degradations to train robust restoration networks. Formally, the mapping from \mathcal{X}_{HQ} to \mathcal{X}_{LQ} is set as,

$$\mathcal{D} : \mathcal{X}_{\text{HQ}} \rightarrow \mathcal{X}_{\text{LQ}} \quad (2)$$

where \mathcal{D} is modeled as a compounded function of random degradations. However, existing methods still face significant challenges when confronted with Extreme Blind Image Restoration (EBIR), where the input image suffers from exceptionally severe and compounded degradations *beyond the scales of their original training settings*.

In EBIR, the combined effect of severe degradation and their blind, random composition causes the domain gap between \mathcal{X}_{HQ} and the space of ELQ images \mathcal{X}_{ELQ} to become *massive*. Denoting the mapping from \mathcal{X}_{ELQ} to \mathcal{X}_{HQ} as follows,

$$\mathcal{R}_E : \mathcal{X}_{\text{ELQ}} \rightarrow \mathcal{X}_{\text{HQ}} \quad (3)$$

A trivial approach such as learning \mathcal{R}_E end-to-end with a single model would lead to suboptimal results due to the highly complex transformation and intractably large solution space. The network would struggle in learning a stable and effective mapping, producing outputs with unnatural textures or failing to recover essential structural details. To address this challenge, we factorize the mapping \mathcal{R}_E into two simpler sub-problems. Specifically, instead of learning \mathcal{R}_E directly, we first project an ELQ image onto an intermediate LQ manifold via a trainable projector $f_\theta : \mathcal{X}_{\text{ELQ}} \rightarrow \mathcal{X}_{\text{LQ}}$, and then apply a frozen pretrained restoration model $g : \mathcal{X}_{\text{LQ}} \rightarrow \mathcal{X}_{\text{HQ}}$. Such decomposition of \mathcal{R}_E into a $\mathcal{X}_{\text{ELQ}} \rightarrow \mathcal{X}_{\text{LQ}} \rightarrow \mathcal{X}_{\text{HQ}}$ path effectively shrinks the solution space via an intermediate distribution and stabilizes learning in the severe, compound-degradation regime.

We ground the design of our method by a novel perspective of the image restoration task as an **Information Bottleneck (IB)** problem (Tishby et al., 2000; Tishby & Zaslavsky, 2015; Alemi et al., 2016), originally designed for the *compression* of one random variable while maintaining the *relevance* of another. We reframe the task of image restoration by introducing a *degrade-back* simulation for $\mathcal{X}_{\text{LQ}} \rightarrow \mathcal{X}_{\text{HQ}} \dashrightarrow \mathcal{X}_{\text{LQ}}$, and regarding a reconstructed HQ image as a *compressed* form of the given LQ image in terms of degradation and artifacts. Importantly, this perspective provides a theoretically-driven objective consisting of an LQ reconstruction term and an HQ prior-matching term. Formally, we derive the *Image Restoration Information Bottleneck (IRIB) loss* and its variant for training f_θ to restore ELQ images with a fixed pretrained $\mathcal{X}_{\text{LQ}} \rightarrow \mathcal{X}_{\text{HQ}}$ mapping network g .

The proposed decomposition of the IR task also enables application of auxiliary refinement methods during inference time. Our pipeline exposes an intermediate space \mathcal{X}_{LQ} which serves as an appropriate location for refinement. Specifically, we introduce **Look Forward Once (LFO)**¹ to refine conditioning (e.g., text prompts) using intermediate samples before finally mapping to an HQ

¹Name inspired by the work Zhang et al. (2022).

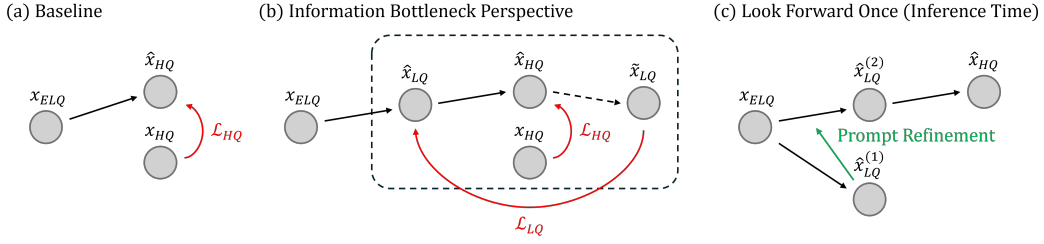


Figure 2: **(a) Baseline Methods:** Conventional restoration learns a single mapping $\mathcal{X}_{ELQ} \rightarrow \mathcal{X}_{HQ}$ from Extreme LQ images to HQ images. This is a highly ill-posed problem, thus training with only the HQ matching objective \mathcal{L}_{HQ} becomes highly impractical. **(b) Our Information Bottleneck Perspective** introduces an intermediate distribution \mathcal{X}_{LQ} and simulates a *degrade-back* channel, leading to an additional LQ reconstruction objective \mathcal{L}_{LQ} . **(c) Look Forward Once (LFO):** The decomposition of the $\mathcal{X}_{ELQ} \rightarrow \mathcal{X}_{HQ}$ problem to $\mathcal{X}_{ELQ} \rightarrow \mathcal{X}_{LQ} \rightarrow \mathcal{X}_{HQ}$ allows for auxiliary refinement in the intermediate LQ distribution during inference time. Prompt refinement via LFO improves performance of extreme image restoration by finding a finer image in the LQ domain.

image. This method can be used *iteratively* to enhance performance during inference time with minimal overhead. Furthermore, a well-trained projection $f_\theta : \mathcal{X}_{ELQ} \rightarrow \mathcal{X}_{LQ}$ would allow us to leverage f_θ to enhance the restoration properties of *any* pretrained image restoration model $g : \mathcal{X}_{LQ} \rightarrow \mathcal{X}_{HQ}$, provided that the subspace \mathcal{X}_{LQ} is identical. In fact, many state-of-the-art IR methods are trained with the same degradation \mathcal{D} ; our method proves effective for broadening the restoration capabilities of pretrained BIR models up to *extreme* BIR in a plug-and-play fashion without training.

In summary, our contributions are as follows:

- We recast extreme blind image restoration as an Information Bottleneck (IB) problem and derive the Image Restoration Information Bottleneck (IRIB) objective that couples an LQ reconstruction term with an HQ prior-matching term.
- We introduce a decomposition of the Extreme Blind Image Restoration problem, and an efficient method for solving it leveraging the IRIB objective. Such decomposition shrinks the solution space, enabling efficient training while producing realistic high-quality results.
- Our framework enables Look Forward Once, a strategy for inference-time prompt refinement that can be iteratively applied, and plug-and-play strengthening of existing image restoration models without need for finetuning.

2 RELATED WORK

Blind Image Restoration. Blind image restoration (BIR) aims to restore images degraded by \mathcal{D}_ϕ without knowledge of ϕ . In real-world scenarios, we do not have knowledge of both \mathcal{D} and ϕ , causing the IR task to be *fully blind*. Although solving fully blind IR allows for more practical use cases, the intensified ill-posedness induces additional difficulties. Random-degradation training has become a practical recipe for solving fully blind IR: BSRGAN (Zhang et al., 2021) designs a shuffled, multi-stage degradation pipeline to synthesize diverse low-quality inputs for training, and Real-ESRGAN Wang et al. (2021) incorporates higher-order degradations. By virtue of such powerful training pipelines, recent BIR models are now capable of producing remarkable results (Wu et al., 2024b; Wang et al., 2024; Sun et al., 2025; Wu et al., 2024a; Lin et al., 2024). Among them, DiffBIR (Lin et al., 2024) casts blind restoration as a two-stage pipeline by conditioning a latent diffusion prior with region-adaptive guidance. SeeSR (Wu et al., 2024b) uses semantic prompts to restore images, but its diffusion-based nature demands high inference time. OSEDiff (Wu et al., 2024a) replaces multi-step diffusion sampling with a one-step diffusion-based generator stabilized by variational score distillation. A major challenge for all pretrained BIR models is that, once trained, *they cannot be leveraged to restore images of degradations beyond their training regime*. This is a critical drawback, as the additional training incurred is non-trivial due to the severe ill-posedness of the problem. Thus, we propose to *decompose* the image restoration process to mitigate the ill-posedness by introducing an intermediate distribution of less degradation. Leveraging a theoretically driven loss, our method enables successful restoration even for extremely degraded images.

Decomposition of Image Restoration. A long line of image restoration methods reduces ill-posedness by inserting intermediate states that progressively constrain the solution. Pyramidal designs reconstruct at multiple resolutions (*e.g.*, progressive Laplacian pyramid of LapSRN (Lai et al., 2017), multi-scale deblurring via coarse-to-fine updates (Nah et al., 2017)), and CinCGAN (Yuan et al., 2018) bridges to a cleaner LR domain before upscaling. GAN-prior methods such as GLEAN (Chan et al., 2021) and PULSE (Menon et al., 2020) search or bank latent codes as an intermediate manifold. Recent two-stage pipelines (DiffBIR (Lin et al., 2024), SeeSR (Wu et al., 2024b)) first move inputs to a cleaner intermediate (degradation-removed or semantics-aligned) state, then invoke a powerful diffusion prior for detail synthesis. Chain-of-Zoom (Kim et al., 2025) attempts a similar decomposition of the super-resolution task for extreme super-resolution during inference time. However, these methods do not solve the problem of restoring from extremely low-quality inputs under compounded, unknown degradations, where learning a direct mapping to high quality remains ill-posed. Instead of proxy scales/latents or denoise-then-regenerate stages, our method inserts a low-quality intermediate distribution aligned with real degradations and trains a projection module to populate it while the restoration backbone remains frozen.

3 PRELIMINARIES

The Information Bottleneck. Let $(X, Y) \sim p(x, y)$. The Information Bottleneck (IB) principle seeks a stochastic representation Z of X that keeps only task-relevant information about Y while compressing X (Tishby et al., 2000; Tishby & Zaslavsky, 2015). The IB seeks to minimize

$$\min_{p(z|x)} \mathcal{L}_{\text{IB}} := I(X; Z) - \beta I(Z; Y), \quad \beta > 0. \quad (4)$$

Minimizing the compression term $I(X; Z)$ enforces compression, forcing the representation Z to discard information irrelevant to the task. Maximizing the relevance term $I(Z; Y)$ ensures that the representation Z remains useful for predicting the target Y .

The Variational Information Bottleneck. A primary obstacle to the direct application of the IB principle in deep learning is the computational intractability of mutual information. The Deep Variational Information Bottleneck (VIB) (Alemi et al., 2016) provides a practical solution by deriving a tractable variational lower bound on the IB objective. This bound can be readily optimized using standard stochastic gradient-based methods. Formally, a parametric encoder $q_\phi(z|x)$, decoder $q_\psi(y|z)$, and a simple variational prior $r(z)$ (*e.g.*, $\mathcal{N}(0, I)$) is introduced to bound the two mutual information terms $I(X; Z)$ and $I(Z; Y)$.

An upper bound on $I(X; Z)$ is derived as follows:

$$\begin{aligned} I(X; Z) &= \mathbb{E}_{p(x,z)} [\log q_\phi(z|x) - \log p(z)] \\ &\leq \mathbb{E}_{p(x,z)} [\log q_\phi(z|x) - \log r(z)] = \mathbb{E}_{p(x)} [\text{KL}(q_\phi(z|x) \parallel r(z))] \end{aligned} \quad (5)$$

where the inequality comes from $\text{KL}(p(z) \parallel r(z)) \geq 0 \Rightarrow \mathbb{E} \log p(z) \geq \mathbb{E} \log r(z)$. Similarly, a lower bound on $I(Z; Y)$ is derived as follows:

$$I(Z; Y) = \mathbb{E}_{p(y,z)} [\log p(y|z)] - \mathbb{E}_{p(y)} [\log p(y)] \geq \mathbb{E}_{p(x,y)} \mathbb{E}_{q_\phi(z|x)} [\log q_\psi(y|z)] + H(Y), \quad (6)$$

where the inequality comes from $\text{KL}(p(y|z) \parallel q_\psi(y|z)) \geq 0 \Rightarrow \mathbb{E} \log p(y|z) \geq \mathbb{E} \log q_\psi(y|z)$. The $H(Y)$ term is constant with respect to model parameters in supervised setups. Combining the bounds in the IB Lagrangian of Eq. 4, the following holds:

$$\mathcal{L}_{\text{IB}} \leq \underbrace{\mathbb{E}_{p(x)} [\text{KL}(q_\phi(z|x) \parallel r(z))]}_{\text{compression term}} - \beta \underbrace{\mathbb{E}_{p(x,y)} \mathbb{E}_{q_\phi(z|x)} [\log q_\psi(y|z)]}_{\text{relevance term}} + \text{const.} \quad (7)$$

Thus, minimizing the upper bound of Eq. (7) is equivalent to minimizing the VIB loss

$$\mathcal{L}_{\text{VIB}}(\phi, \psi) = \mathbb{E}_{p(x,y)} [\mathbb{E}_{q_\phi(z|x)} [-\log q_\psi(y|z)] + \beta \text{KL}(q_\phi(z|x) \parallel r(z))]. \quad (8)$$

Connection to β -VAE. Setting the IB relevant variable to the input itself ($Y = X$; self-prediction) and using the same variational family as in VIB, we obtain the β -VAE loss:

$$\mathcal{L}_{\beta\text{-VAE}}(\phi, \psi) = \mathbb{E}_{p(x)} [\mathbb{E}_{q_\phi(z|x)} [-\log q_\psi(x|z)] + \beta \text{KL}(q_\phi(z|x) \parallel r(z))]. \quad (9)$$

In this work, we redefine the problem of image restoration in the lens of the Information Bottleneck principle, and propose a theoretically-driven method for effectively solving extreme image restoration with pretrained image restoration models.

4 EXTREME IMAGE RESTORATION AS AN INFORMATION BOTTLENECK

4.1 OVERVIEW

Let $X \sim p_{\text{LQ}}$ be low-quality (LQ) images and $Z \sim p_{\text{HQ}}$ be high-quality (HQ) images. Baseline methods for image restoration aim to find an effective mapping $g : \mathcal{X}_{\text{LQ}} \rightarrow \mathcal{X}_{\text{HQ}}$:

$$\underbrace{X}_{\text{LQ}} \xrightarrow{g} \underbrace{Z}_{\text{HQ proxy}}, \quad \text{with } Z \in \mathcal{X}_{\text{HQ}}. \quad (10)$$

In this work, we present a novel perspective of the image restoration problem as an Information Bottleneck (IB) problem via simulating the *degrade-back* of an HQ proxy:

$$\underbrace{X}_{\text{LQ}} \xrightarrow{g} \underbrace{Z}_{\text{HQ proxy}} \xrightarrow{d_\psi} \tilde{X}, \quad \text{with } Z \in \mathcal{X}_{\text{HQ}}, \tilde{X} \in \mathcal{X}_{\text{LQ}}. \quad (11)$$

where $d_\psi : \mathcal{X}_{\text{HQ}} \rightarrow \mathcal{X}_{\text{LQ}}$ is a possible degradation channel. This shows strong correspondence to the self-prediction case (*i.e.*, β -VAE) of the Variational Information Bottleneck, allowing us to directly leverage the β -VAE loss of Eq. (9) to formulate the **Image Restoration Information Bottleneck (IRIB)** loss:

$$\mathcal{L}_{\text{IRIB}}(\phi, \psi) = \mathbb{E}_{p(x)} \left[\underbrace{\mathbb{E}_{q_\phi(z|x)} [-\log q_\psi(x|z)]}_{\mathcal{L}_{\text{LQ-recon}}} + \beta \underbrace{\text{KL}(q_\phi(z|x) \parallel r(z))}_{\mathcal{L}_{\text{HQ-prior}}} \right]. \quad (12)$$

where $q_\psi(x|z)$ parameterizes the LQ-likelihood induced by d_ψ . Note that this loss mirrors that of β -VAE exactly: a reconstruction term and a prior matching term.

Information Bottleneck for Extreme Image Restoration. Given the loss $\mathcal{L}_{\text{IRIB}}$, we now propose a novel method for using it to solve the problem of extreme image restoration. Specifically, we aim to leverage a *pretrained* mapping g and leverage it to solve restoration tasks for extremely low-quality images that are degraded beyond the training configuration of g . Let $X^{(E)} \sim p_{\text{ELQ}}$ be extremely low-quality (ELQ) images. We aim to find an effective mapping $f_\theta : \mathcal{X}_{\text{ELQ}} \rightarrow \mathcal{X}_{\text{LQ}}$:

$$\underbrace{X^{(E)}}_{\text{ELQ}} \xrightarrow{f_\theta} \underbrace{\hat{X}}_{\text{LQ proxy}} \xrightarrow{g} \underbrace{\hat{Z}}_{\text{HQ proxy}} \xrightarrow{d_\psi} \tilde{X}, \quad \text{with } \hat{Z} \in \mathcal{X}_{\text{HQ}}, \hat{X} \in \mathcal{X}_{\text{LQ}}, \tilde{X} \in \mathcal{X}_{\text{LQ}}. \quad (13)$$

Since a naive mapping to directly learn $\mathcal{X}_{\text{ELQ}} \rightarrow \mathcal{X}_{\text{HQ}}$ would impose impractical training costs and suboptimal results, we leverage the proposed IRIB loss *to introduce an LQ proxy* for restricting the solution space in an intermediate distribution. The IRIB loss of Eq. (12) thus becomes:

$$\begin{aligned} & \mathcal{L}_{\text{IRIB-ELQ}}(\theta; \phi, \psi) \\ &= \mathbb{E}_{(x^{(E)}, x) \sim p_{\text{ELQ}, \text{LQ}}} \left[\underbrace{\mathbb{E}_{q_\phi(z|f_\theta(x^{(E)}))} [-\log q_\psi(x|z)]}_{\mathcal{L}_{\text{LQ-recon}}} + \beta \underbrace{\text{KL}(q_\phi(z|f_\theta(x^{(E)})) \parallel r(z))}_{\mathcal{L}_{\text{HQ-prior}}} \right]. \end{aligned} \quad (14)$$

where the optimization is with respect to θ .

4.2 TRAINING OBJECTIVE

The proposed loss $\mathcal{L}_{\text{IRIB-ELQ}}$ provides a simple method to solve image restoration tasks in extreme low-quality settings with minimal training. We now show how this loss is used as a practical training loss by examining each of its terms in detail.

LQ reconstruction term. For a given random degradation \mathcal{D} , we set $q_\psi(x|z) = \mathcal{N}(\mathcal{D}(z), \sigma^2 I)$, which yields the LQ reconstruction loss as:

$$\mathcal{L}_{\text{LQ-recon}} = \mathbb{E}_{p(x)q_\phi(z|x)} \left[\frac{1}{2\sigma^2} \|\mathcal{D}(z) - x\|_2^2 \right] + \text{const}. \quad (15)$$

The LQ reconstruction loss minimizes the ℓ_2 distance of LQ image x to the randomly degraded image $\mathcal{D}(z)$. However, a plain pixelwise ℓ_2 objective disproportionately penalizes high-frequency discrepancies. This is ill-suited to our setting because \mathcal{D} typically contains downsampling that discard

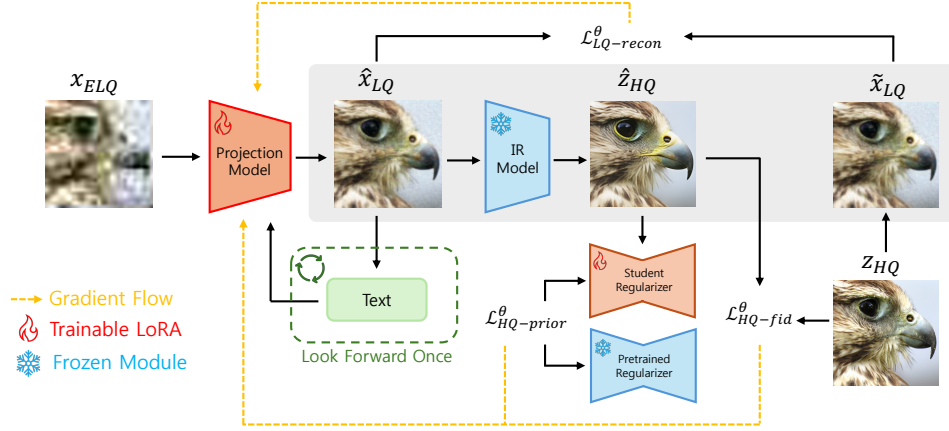


Figure 3: **Overall Pipeline.** Given an ELG image x_{ELQ} , the trainable projector f_θ produces \hat{x}_{LQ} ; a frozen restoration model g outputs \hat{z}_{HQ} . We simulate the *degrade-back* to obtain $\tilde{x}_{LQ} = \mathcal{D}(z_{HQ})$ and minimize a blur-aware LQ reconstruction loss $\mathcal{L}_{LQ-recon}$. To regularize toward the HQ distribution, we apply $\mathcal{L}_{HQ-prior}$ and \mathcal{L}_{HQ-fid} . Gradients for the terms only flow through f_θ while g and the prior remain frozen. Recursive prompt refinement can condition f_θ/g during inference time, enabling Look Forward Once refinement.

high-frequency details; as a result, multiple valid realizations of $\mathcal{D}(z)$ can differ in high-frequency content while being perceptually and semantically equivalent at LQ.

To improve robustness, we compare signals after a shared low-pass transform. Let G_τ denote a Gaussian blur operator with standard deviation τ . We define the *blur-MSE* loss

$$\mathcal{L}_{LQ-recon} = \mathbb{E}_{p(x)q_\phi(z|x)} \left[\frac{1}{2\sigma^2} \| G_\tau * \mathcal{D}(z) - G_\tau * x \|_2^2 \right], \quad (16)$$

where the same Gaussian kernel G_τ is applied to both $\mathcal{D}(z)$ and x . In the frequency domain, (16) weights discrepancies by down weighting high frequency mismatches that \mathcal{D} cannot reliably preserve and attenuating noise-induced fluctuations.

In our practical implementation, the degradation \mathcal{D} is set as that of the Real-ESRGAN pipeline (Wang et al., 2021). This degradation is shared among many state-of-the-art image restoration models; hence we can apply the trained f_θ to broaden the applicability of various different image restoration models. We examine the detailed effects in our experiments.

HQ prior matching term. We match $q_\phi(z|x)$ to an HQ prior $r(z) \approx p_{HQ}$ for the prior matching term $\mathcal{L}_{HQ-prior}$. Though this can be performed in many different ways (e.g., adversarial loss, variational score distillation, f-divergence), for the context of image restoration we leverage the following prior matching loss originated from diffusion models:

$$\mathcal{L}_{HQ-prior} = \mathbb{E}_{x \sim p(x)q_\phi(z|x), \epsilon \sim \mathcal{N}(0, I)} \left[\frac{1}{2} \|\hat{\epsilon}(z_t, t) - \hat{\epsilon}_{HQ}(z_t, t)\|_2^2 \right]. \quad (17)$$

Here, $\hat{\epsilon}$ is the student noise predictor and $\hat{\epsilon}_{HQ}$ is the (fixed) HQ prior’s noise predictor, both evaluated on the same noised latent z_t .

Beyond prior matching, we enforce sample-wise fidelity to the paired HQ target. We combine pixel, perceptual, and blur-aware terms:

$$\mathcal{L}_{HQ-fid} = \mathbb{E}_{(x,y), z \sim q_\phi(z|x)} \left[\lambda_{l2} \|\hat{z} - z\|_2^2 + \lambda_{LPIPS} \text{LPIPS}(\hat{z}, z) + \lambda_{blur} \| G_k * \hat{z} - G_k * z \|_2^2 \right], \quad (18)$$

where G_k is a Gaussian blur operator applied symmetrically to both images. In this case, the *blur-MSE* term acts as a robustness prior in the HQ domain. When the input is extremely degraded, multiple plausible restorations can share low-frequency structure while differing in fine details. Allowing this controlled freedom via λ_{blur} and kernel size k offers more realistic outputs with a small trade-off in pixel fidelity.

The total loss w.r.t. the network parameter θ becomes:

$$\mathcal{L}_{total} = \mathcal{L}_{LQ-recon} + \mathcal{L}_{HQ-prior} + \mathcal{L}_{HQ-fid}. \quad (19)$$

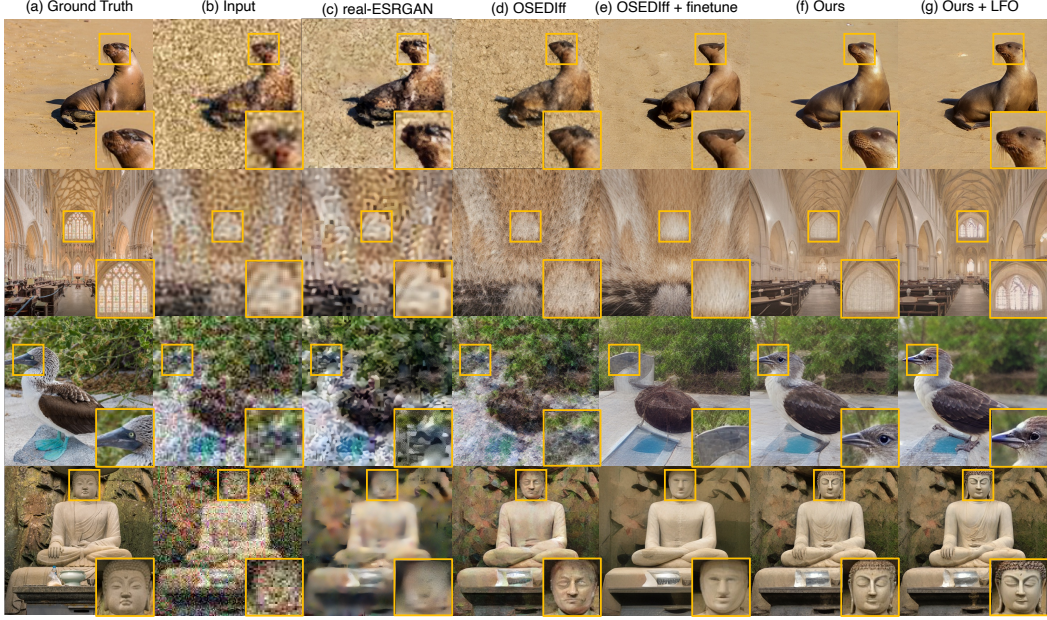


Figure 4: **Qualitative Comparison.** (c-d) One step restoration of OSEDIff and its finetuned model; (e-g) Our methods and LFO prompt refinement variants. Although the fine-tuned OSEDIff improves image quality over the naïve baseline, it still produces occasional unrealistic artifacts. In contrast, the IRIB framework (ours) yields restorations that are both realistic and consistent with the ELQ input, effectively recovering the most probable image under severe degradations.

4.3 LOOK FORWARD ONCE

Decomposing the $\mathcal{X}_{\text{ELQ}} \rightarrow \mathcal{X}_{\text{HQ}}$ task to $\mathcal{X}_{\text{ELQ}} \rightarrow \mathcal{X}_{\text{LQ}} \rightarrow \mathcal{X}_{\text{HQ}}$ as in (13) also opens additional venues for refinement that we can exploit *during inference time* for improved restoration performance. In this work, we introduce Look Forward Once, a method for leveraging the LQ proxy \hat{X}_{LQ} to perform auxiliary refinement via text prompt conditioning during inference time.

In our practical setup, the learnable projection model f_θ and the frozen IR model g are both restoration models capable of referring to an input text condition. Let $(x_{\text{ELQ}}, \hat{x}_{\text{LQ}}, \hat{x}_{\text{HQ}})$ denote the given ELQ image, restored LQ image, and restored HQ image, respectively. Also, define c_{ELQ} as the text condition used in f_θ for restoring x_{ELQ} to \hat{x}_{LQ} , and c_{LQ} as the text condition used in g for restoring \hat{x}_{LQ} to \hat{x}_{HQ} . The prompts c_{ELQ} and c_{LQ} are obtained with a prompt extraction module Y as follows:

$$c_{\text{ELQ}} := Y(x_{\text{ELQ}}), \quad c_{\text{LQ}} := Y(\hat{x}_{\text{LQ}}) \quad (20)$$

In the proposed method, given the input x_{ELQ} we *look forward once* during the restoration process to obtain an initial text condition $c_{\text{ELQ}}^{(1)}$ and its corresponding LQ image $\hat{x}_{\text{LQ}}^{(1)}$.

$$c_{\text{ELQ}}^{(1)} = Y(x_{\text{ELQ}}), \quad \hat{x}_{\text{LQ}}^{(1)} = g(f_\theta(x_{\text{ELQ}}; c_{\text{ELQ}}^{(1)})) \quad (21)$$

Then, we leverage $\hat{x}_{\text{LQ}}^{(1)}$ to create an improved text condition $c_{\text{ELQ}}^{(2)}$, which is subsequently used for the *second pass* of $\mathcal{X}_{\text{ELQ}} \rightarrow \mathcal{X}_{\text{LQ}}$. The corresponding $\hat{x}_{\text{LQ}}^{(2)}$ is used for the final $\mathcal{X}_{\text{LQ}} \rightarrow \mathcal{X}_{\text{HQ}}$ process to obtain \hat{x}_{HQ} . The final ELQ-to-HQ restoration process with LFO can be written as:

$$c_{\text{ELQ}}^{(2)} = Y(\hat{x}_{\text{LQ}}^{(1)}), \quad \hat{x}_{\text{HQ}} = g(f_\theta(x_{\text{ELQ}}; c_{\text{ELQ}}^{(2)})) \quad (22)$$

Here, the choice of prompt extraction module Y is flexible (e.g., DAPE (Wu et al., 2024b) or VLM). By utilizing the intermediate successive prompts amidst the ELQ-to-HQ restoration process, we are able to provide better conditioning to be used for the ELQ-to-LQ restoration.

Table 1: Quantitative comparison. **Bold**: best, Underline: second-best.

DIV2K										
Method	Training Type	LFO	PSNR \uparrow	SSIM \uparrow	LPIPS \downarrow	DISTS \downarrow	FID \downarrow	NIQE \downarrow	MUSIQ \uparrow	CLIPQA \uparrow
Real-ESRGAN	Pretrained	\times	19.5666	0.4360	0.7020	0.3875	159.1040	8.6893	31.7782	0.3595
OSDiff	Pretrained	\times	19.6772	0.4397	0.4848	0.3029	81.5558	4.3314	63.8965	0.6202
OSDiff	ELQ \rightarrow HQ	\times	20.0958	0.4818	0.4275	0.2710	68.0802	4.1018	69.9307	0.6615
OSDiff + Ours	ELQ \rightarrow LQ \rightarrow HQ	\times	<u>20.0488</u>	<u>0.4797</u>	<u>0.4249</u>	0.2621	<u>62.9768</u>	<u>4.1814</u>	70.3529	0.6829
OSDiff + Ours	ELQ \rightarrow LQ \rightarrow HQ	$\times 1$	20.0084	0.4790	0.4261	<u>0.2599</u>	63.1425	4.1830	<u>70.6405</u>	<u>0.6844</u>
OSDiff + Ours	ELQ \rightarrow LQ \rightarrow HQ	$\times 2$	20.0047	0.4790	0.4255	0.2594	62.9475	4.1875	70.6806	0.6848

DIV8K										
Method	Training Type	LFO	PSNR \uparrow	SSIM \uparrow	LPIPS \downarrow	DISTS \downarrow	FID \downarrow	NIQE \downarrow	MUSIQ \uparrow	CLIPQA \uparrow
Real-ESRGAN	Pretrained	\times	20.2318	0.4508	0.7096	0.3800	144.1936	8.6526	32.3691	0.3721
OSDiff	Pretrained	\times	20.5186	0.4651	0.4710	0.2944	58.1913	4.5441	63.9930	0.6309
OSDiff	ELQ \rightarrow HQ	\times	20.9333	0.5065	0.4082	0.2627	43.5674	4.2649	69.3240	0.6560
OSDiff + Ours	ELQ \rightarrow LQ \rightarrow HQ	\times	20.8791	0.5040	0.4051	0.2535	40.7901	4.3803	69.7483	<u>0.6803</u>
OSDiff + Ours	ELQ \rightarrow LQ \rightarrow HQ	$\times 1$	20.8489	0.5038	0.4057	<u>0.2516</u>	<u>40.5819</u>	4.3829	<u>69.8903</u>	0.6801
OSDiff + Ours	ELQ \rightarrow LQ \rightarrow HQ	$\times 2$	20.8421	0.5039	<u>0.4053</u>	0.2505	40.5523	<u>4.3719</u>	70.0020	0.6806

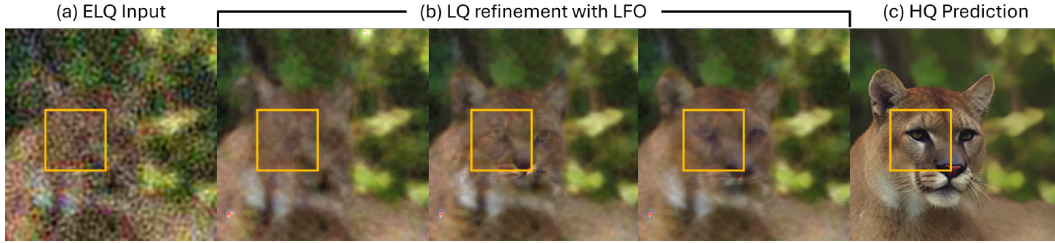


Figure 5: **LQ refinement with LFO.** (a) The ELQ input. (b) From left to right: the initial LQ sample; the refined LQ sample after $1 \times$ LFO; the refined LQ sample after $2 \times$ LFO. Iterative refinement of the LQ sample with LFO forms coarse structure (*e.g.*, eye) in LQ. (c) The final HQ output.

5 EXPERIMENTS

5.1 EXPERIMENTAL SETTINGS

We train at 512×512 resolution on the LSDIR dataset (Li et al., 2023). Both projection model and frozen IR model follow OSDiff, with backbone Stable Diffusion v2.1 (Wu et al., 2024a). We extract image tags with RAM (Zhang et al., 2024b) as prompts; for unreliable tagging due to severe degradation, we apply prompt dropout by using a null prompt with probability 0.3 for improved robustness. Synthetic degradations follow the Real-ESRGAN pipeline (Wang et al., 2021): our LQ setting uses the default configuration, while the extreme-LQ setting widens ranges for resizing factors, blur kernels (Gaussian σ / generalized-Gaussian β), additive noise, and JPEG quality. We fine-tune only LoRA adapters of rank 4 with learning rate 5×10^{-5} on $4 \times$ A100 GPUs. For testing, we evaluate our model on DIV2K and DIV8K train sets (800 and 1,500 images, respectively). All images are resized and center-cropped to 512×512 resolution. At test time, the same degradation settings as for training are applied and DAPE Wu et al. (2024b) is used for prompt extraction.

5.2 COMPARISON RESULTS

We compare our IRIB setting against one-step IR models; real-ESRGAN, OSDiff, and OSDiff trained under the same extreme-degradation configuration. Our method employs LFO to iteratively extract prompts from intermediate LQ images to further refine the output.

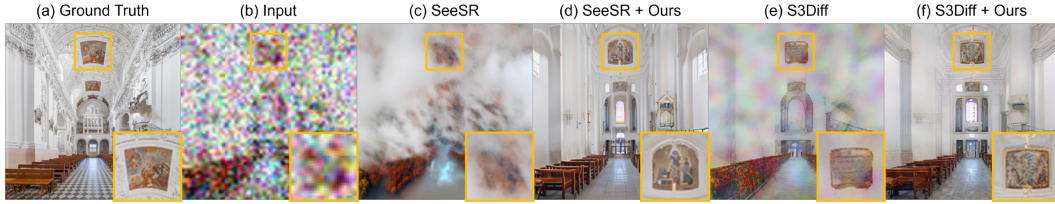
Qualitative Comparison. Qualitative comparison is depicted in Figure 4. The naïve OSDiff, trained solely on LQ images, struggles to recover severely degraded inputs and leaves noticeable artifacts. The fine-tuned OSDiff improves visual quality but still exhibits irregular deformations and hallucinated textures. In contrast, combining an explicit projection onto the LQ manifold with LFO refinement restores ELQ inputs to semantically plausible, realistic images with higher fidelity.

Quantitative Comparison. Quantitative results are given in Table 1, and ablation study provided in Appendix A. We use PSNR, SSIM, LPIPS (Zhang et al., 2018), DISTS for fidelity metrics and NIQE (Zhang et al., 2015), MUSIQ (Ke et al., 2021), CLIPQA (Wang et al., 2023) for perceptual metrics. To evaluate the realism of the restored images we use Frechet Inception Distance (FID).

Table 2: Plug-and-Play results of our projection module f_θ on existing BIR models. **Bold**: best.

Method	DIV2K							
	PSNR \uparrow	SSIM \uparrow	LPIPS \downarrow	DISTS \downarrow	FID \downarrow	NIQE \downarrow	MUSIQ \uparrow	CLIPQA \uparrow
S3Diff	19.5941	0.4379	0.4583	0.2830	74.7576	4.8987	63.5064	0.6411
S3Diff + Ours	19.8582	0.4581	0.4075	0.2382	58.3893	4.3436	70.8872	0.6975
SeeSR	19.1646	0.4430	0.4738	0.2507	69.3567	4.4721	71.1555	0.7424
SeeSR + Ours	19.9312	0.4632	0.4506	0.2374	61.2615	4.1355	71.5719	0.7320

Method	DIV8K							
	PSNR \uparrow	SSIM \uparrow	LPIPS \downarrow	DISTS \downarrow	FID \downarrow	NIQE \downarrow	MUSIQ \uparrow	CLIPQA \uparrow
S3Diff	20.4950	0.4630	0.4490	0.2754	53.0353	4.9418	62.9439	0.6386
S3Diff + Ours	20.7011	0.4813	0.3880	0.2334	36.7050	4.5596	70.5182	0.6935
SeeSR	20.0719	0.4693	0.4622	0.2476	43.4365	4.6056	70.3421	0.7395
SeeSR + Ours	20.8649	0.4921	0.4345	0.2345	39.6162	4.3091	70.7543	0.7285

Figure 6: **Plug-and-Play with Existing BIR Models.** (c,e) Direct ELQ restoration of baselines; (d,f) LQ restoration of baselines after IRIB projection. Integrating our method enables SeeSR and S3Diff to produce high-fidelity reconstructions from ELQ inputs with little to no hallucination.

Given that severely degraded inputs admit multiple plausible restorations, we prioritize perceptual realism while preserving global structure. Our method produces semantically faithful, visually plausible results with only minor trade-offs in pixel-level fidelity (e.g., PSNR/SSIM). In particular, recursive LFO refinement consistently improves perceptual metrics yielding higher perceived quality.

5.3 PLUG-AND-PLAY WITH EXISTING BASED BIR MODELS

We integrate our $\text{ELQ} \rightarrow \text{LQ}$ projection with existing IR models SeeSR (Wu et al., 2024b) and S3Diff (Zhang et al., 2024a), trained on the same Real-ESRGAN degradation pipeline as our setup. Figure 6 contrasts two pipelines: (i) Directly feeding the ELQ input to the IR model, and (ii) projecting ELQ to the LQ manifold using our method, then applying the IR model for $\text{LQ} \rightarrow \text{HQ}$ restoration. SeeSR and S3Diff is kept frozen and evaluated with the official inference settings. Directly using an IR model for ELQ images exhibits softened details and deformations. In contrast, our method reduces artifacts and recovers sharper, more coherent structures. Quantitatively (Table 2), our method yields substantial improvement across pixel fidelity, perceptual quality, and realism metrics.

6 CONCLUSION

Extreme Blind Image Restoration (EBIR) remains under-explored. We introduce an EBIR framework cast in the Information Bottleneck (IB) paradigm, deriving the *Image Restoration Information Bottleneck* (IRIB) objective that couples a blur-aware LQ reconstruction term with an HQ prior-matching term, optionally complemented by sample-wise HQ fidelity losses. By factorizing restoration into an $\text{ELQ} \rightarrow \text{LQ} \rightarrow \text{HQ}$ pipeline and training only a projector f_θ while reusing a frozen backbone g , we shrink the search space, stabilize optimization under compounded degradations, and expose an intermediate LQ representation that enables *Look Forward Once* (LFO) prompt refinement. Our framework is modular thus providing broad applicability; existing BIR models (i.e., SeeSR, S3Diff) can be improved in a plug-and-play setting. Future work includes learning degradations beyond Real-ESRGAN and extending to additional modalities to enhance generalization.

Limitations. One limitation of our framework is that the pretrained IR model g used for training the f_θ projection must be a single step model for practical usage, since gradients would have to flow through the model multiple times for a multi-step model (e.g., diffusion-based). Furthermore, the prompt extraction module Y is not able to produce optimal results for input ELQ cases. Thus, future work could perform additional fine-tuning of Y or leverage VLMs to achieve higher performance.

REFERENCES

- Alexander A Alemi, Ian Fischer, Joshua V Dillon, and Kevin Murphy. Deep variational information bottleneck. *arXiv preprint arXiv:1612.00410*, 2016.
- Kelvin CK Chan, Xintao Wang, Xiangyu Xu, Jinwei Gu, and Chen Change Loy. Glean: Generative latent bank for large-factor image super-resolution. In *Proceedings of the IEEE/CVF conference on computer vision and pattern recognition*, pp. 14245–14254, 2021.
- Xiangyu Chen, Xintao Wang, Jiantao Zhou, Yu Qiao, and Chao Dong. Activating more pixels in image super-resolution transformer. In *Proceedings of the IEEE/CVF conference on computer vision and pattern recognition*, pp. 22367–22377, 2023.
- Hamadi Chihoui and Paolo Favaro. Invert2restore: Zero-shot degradation-blind image restoration, 2025. URL <https://arxiv.org/abs/2503.21486>.
- Hamadi Chihoui, Abdelhak Lemkhenter, and Paolo Favaro. Blind image restoration via fast diffusion inversion. *arXiv preprint arXiv:2405.19572*, 2024.
- Chao Dong, Chen Change Loy, Kaiming He, and Xiaoou Tang. Learning a deep convolutional network for image super-resolution. In *Computer Vision–ECCV 2014: 13th European Conference, Zurich, Switzerland, September 6–12, 2014, Proceedings, Part IV 13*, pp. 184–199. Springer, 2014.
- Junjie Ke, Qifei Wang, Yilin Wang, Peyman Milanfar, and Feng Yang. Musiq: Multi-scale image quality transformer. In *Proceedings of the IEEE/CVF international conference on computer vision*, pp. 5148–5157, 2021.
- Bryan Sangwoo Kim, Jeongsol Kim, and Jong Chul Ye. Chain-of-zoom: Extreme super-resolution via scale autoregression and preference alignment. *arXiv preprint arXiv:2505.18600*, 2025.
- Wei-Sheng Lai, Jia-Bin Huang, Narendra Ahuja, and Ming-Hsuan Yang. Deep laplacian pyramid networks for fast and accurate super-resolution. In *Proceedings of the IEEE conference on computer vision and pattern recognition*, pp. 624–632, 2017.
- Yawei Li, Kai Zhang, Jingyun Liang, Jiezhang Cao, Ce Liu, Rui Gong, Yulun Zhang, Hao Tang, Yun Liu, Denis Demandolx, et al. Lsdir: A large scale dataset for image restoration. In *Proceedings of the IEEE/CVF Conference on Computer Vision and Pattern Recognition*, pp. 1775–1787, 2023.
- Jingyun Liang, Jiezhang Cao, Guolei Sun, Kai Zhang, Luc Van Gool, and Radu Timofte. Swinir: Image restoration using swin transformer. In *Proceedings of the IEEE/CVF International Conference on Computer Vision*, pp. 1833–1844, 2021.
- Xinqi Lin, Jingwen He, Ziyang Chen, Zhaoyang Lyu, Bo Dai, Fanghua Yu, Yu Qiao, Wanli Ouyang, and Chao Dong. Diffbir: Toward blind image restoration with generative diffusion prior. In *European conference on computer vision*, pp. 430–448. Springer, 2024.
- Sachit Menon, Alexandru Damian, Shijia Hu, Nikhil Ravi, and Cynthia Rudin. Pulse: Self-supervised photo upsampling via latent space exploration of generative models. In *Proceedings of the IEEE/CVF conference on computer vision and pattern recognition*, pp. 2437–2445, 2020.
- Seungjun Nah, Tae Hyun Kim, and Kyoung Mu Lee. Deep multi-scale convolutional neural network for dynamic scene deblurring. In *Proceedings of the IEEE conference on computer vision and pattern recognition*, pp. 3883–3891, 2017.
- Lingchen Sun, Rongyuan Wu, Zhiyuan Ma, Shuaizheng Liu, Qiaosi Yi, and Lei Zhang. Pixel-level and semantic-level adjustable super-resolution: A dual-lora approach. In *Proceedings of the Computer Vision and Pattern Recognition Conference*, pp. 2333–2343, 2025.
- Naftali Tishby and Noga Zaslavsky. Deep learning and the information bottleneck principle. In *2015 IEEE information theory workshop (ITW)*, pp. 1–5. Ieee, 2015.
- Naftali Tishby, Fernando C Pereira, and William Bialek. The information bottleneck method. *arXiv preprint physics/0004057*, 2000.

- Jianyi Wang, Kelvin CK Chan, and Chen Change Loy. Exploring clip for assessing the look and feel of images. In *Proceedings of the AAAI conference on artificial intelligence*, volume 37, pp. 2555–2563, 2023.
- Jianyi Wang, Zongsheng Yue, Shangchen Zhou, Kelvin CK Chan, and Chen Change Loy. Exploiting diffusion prior for real-world image super-resolution. *International Journal of Computer Vision*, 132(12):5929–5949, 2024.
- Xintao Wang, Liangbin Xie, Chao Dong, and Ying Shan. Real-esrgan: Training real-world blind super-resolution with pure synthetic data. In *Proceedings of the IEEE/CVF international conference on computer vision*, pp. 1905–1914, 2021.
- Zhendong Wang, Xiaodong Cun, Jianmin Bao, Wengang Zhou, Jianzhuang Liu, and Houqiang Li. Uformer: A general u-shaped transformer for image restoration. In *Proceedings of the IEEE/CVF conference on computer vision and pattern recognition*, pp. 17683–17693, 2022.
- Rongyuan Wu, Lingchen Sun, Zhiyuan Ma, and Lei Zhang. One-step effective diffusion network for real-world image super-resolution. *Advances in Neural Information Processing Systems*, 37: 92529–92553, 2024a.
- Rongyuan Wu, Tao Yang, Lingchen Sun, Zhengqiang Zhang, Shuai Li, and Lei Zhang. Seesr: Towards semantics-aware real-world image super-resolution. In *Proceedings of the IEEE/CVF conference on computer vision and pattern recognition*, pp. 25456–25467, 2024b.
- Jie Xiao, Ruili Feng, Han Zhang, Zhiheng Liu, Zhantao Yang, Yurui Zhu, Xueyang Fu, Kai Zhu, Yu Liu, and Zheng-Jun Zha. Dreamclean: Restoring clean image using deep diffusion prior. In *The Twelfth International Conference on Learning Representations*, 2024. URL <https://openreview.net/forum?id=6ALuy19mPa>.
- Yuan Yuan, Siyuan Liu, Jiawei Zhang, Yongbing Zhang, Chao Dong, and Liang Lin. Unsupervised image super-resolution using cycle-in-cycle generative adversarial networks. In *Proceedings of the IEEE conference on computer vision and pattern recognition workshops*, pp. 701–710, 2018.
- Syed Waqas Zamir, Aditya Arora, Salman Khan, Munawar Hayat, Fahad Shahbaz Khan, and Ming-Hsuan Yang. Restormer: Efficient transformer for high-resolution image restoration. In *Proceedings of the IEEE/CVF conference on computer vision and pattern recognition*, pp. 5728–5739, 2022.
- Aiping Zhang, Zongsheng Yue, Renjing Pei, Wenqi Ren, and Xiaochun Cao. Degradation-guided one-step image super-resolution with diffusion priors. *arXiv preprint arXiv:2409.17058*, 2024a.
- Hao Zhang, Feng Li, Shilong Liu, Lei Zhang, Hang Su, Jun Zhu, Lionel M Ni, and Heung-Yeung Shum. Dino: Detr with improved denoising anchor boxes for end-to-end object detection. *arXiv preprint arXiv:2203.03605*, 2022.
- Kai Zhang, Wangmeng Zuo, Yunjin Chen, Deyu Meng, and Lei Zhang. Beyond a gaussian denoiser: Residual learning of deep CNN for image denoising. *IEEE transactions on image processing*, 26(7):3142–3155, 2017.
- Kai Zhang, Jingyun Liang, Luc Van Gool, and Radu Timofte. Designing a practical degradation model for deep blind image super-resolution. In *IEEE International Conference on Computer Vision*, pp. 4791–4800, 2021.
- Lin Zhang, Lei Zhang, and Alan C Bovik. A feature-enriched completely blind image quality evaluator. *IEEE Transactions on Image Processing*, 24(8):2579–2591, 2015.
- Richard Zhang, Phillip Isola, Alexei A Efros, Eli Shechtman, and Oliver Wang. The unreasonable effectiveness of deep features as a perceptual metric. In *Proceedings of the IEEE conference on computer vision and pattern recognition*, pp. 586–595, 2018.
- Youcai Zhang, Xinyu Huang, Jinyu Ma, Zhaoyang Li, Zhaochuan Luo, Yanchun Xie, Yuzhuo Qin, Tong Luo, Yaqian Li, Shilong Liu, et al. Recognize anything: A strong image tagging model. In *Proceedings of the IEEE/CVF Conference on Computer Vision and Pattern Recognition*, pp. 1724–1732, 2024b.

A ABLATION STUDY

λ_{blur} ablation study We augment the HQ fidelity objective as in 18 with a blur-MSE term to reflect the ambiguity under extreme degradations: multiple plausible restorations can share similar low-frequency structure while differing in fine details. Concretely, we consider

$$\mathcal{L}_{\text{HQ}}^{\text{blur}} = \lambda_{\text{blur}} \|G_k * \hat{z} - G_k * z\|_2^2 \quad (23)$$

where G_σ is a Gaussian low-pass filter, and ablate $\lambda_{\text{blur}} \in \{0, 0.5, 1, 2\}$ while keeping the λ_{LPIPS} and λ_{L2} fixed to 1. The PSNR-MUSIQ and PSNR-FID plots in Figure 7 visualize the trade-off: as λ_{blur} increases, models move toward higher pixel-level fidelity (PSNR \uparrow) at the expense of perceptual realism and distributional quality (MUSIQ \downarrow , FID \uparrow). Thus, *users are able to freely balance fidelity and perceptual quality as preferred by adjusting λ_{blur}* . Increasing λ_{blur} yields higher fidelity than fine-tuned baselines, but at the cost of perceptual quality. Such effect is monotonic across both DIV2K and DIV8K datasets, with the fine-tuned baseline (*i.e.*, OSEDiff specifically fine-tuned for ELQ \rightarrow LQ mapping) providing an operational reference on these planes. For fair comparison with the baseline we do not apply LFO in our ablations; iteratively applying LFO during inference time further increases performance of our method.

Table 3: Quantitative comparison of varying λ_{blur} compared to a fine-tuned baseline. **Bold**: best.

Method	PSNR \uparrow	SSIM \uparrow	LPIPS \downarrow	DIV2K					CLIPQA \uparrow
				DISTS \downarrow	FID \downarrow	NIQE \downarrow	MUSIQ \uparrow		
OSEDiff Fine-tuned	20.0958	0.4818	0.4275	0.2710	68.0802	4.1018	69.9307		0.6615
OSEDiff + Ours ($\lambda_{\text{blur}} = 0$)	19.5735	0.4300	0.4725	0.3003	62.4275	3.3994	71.1609		0.7004
OSEDiff + Ours ($\lambda_{\text{blur}} = 0.5$)	20.0488	0.4797	0.4249	0.2621	62.9768	4.1814	70.3529		0.6829
OSEDiff + Ours ($\lambda_{\text{blur}} = 1$)	20.1332	0.4838	0.4251	0.2622	63.4009	4.3263	69.5339		0.6753
OSEDiff + Ours ($\lambda_{\text{blur}} = 2$)	20.2779	0.4871	0.4263	0.2644	63.3627	4.4081	68.9951		0.6774

Method	PSNR \uparrow	SSIM \uparrow	LPIPS \downarrow	DIV8K					CLIPQA \uparrow
				DISTS \downarrow	FID \downarrow	NIQE \downarrow	MUSIQ \uparrow		
OSEDiff Fine-tuned	20.9333	0.5065	0.4082	0.2627	43.5674	4.2649	69.3240		0.6560
OSEDiff + Ours ($\lambda_{\text{blur}} = 0$)	20.7544	0.5016	0.4044	0.2510	40.2708	4.2857	70.1484		0.6830
OSEDiff + Ours ($\lambda_{\text{blur}} = 0.5$)	20.8791	0.5040	0.4051	0.2535	40.7899	4.3803	69.7483		0.6803
OSEDiff + Ours ($\lambda_{\text{blur}} = 1$)	20.9850	0.5071	0.4076	0.2554	41.2787	4.4901	69.1095		0.6760
OSEDiff + Ours ($\lambda_{\text{blur}} = 2$)	21.1423	0.5108	0.4075	0.2563	41.4256	4.5464	68.5735		0.6783

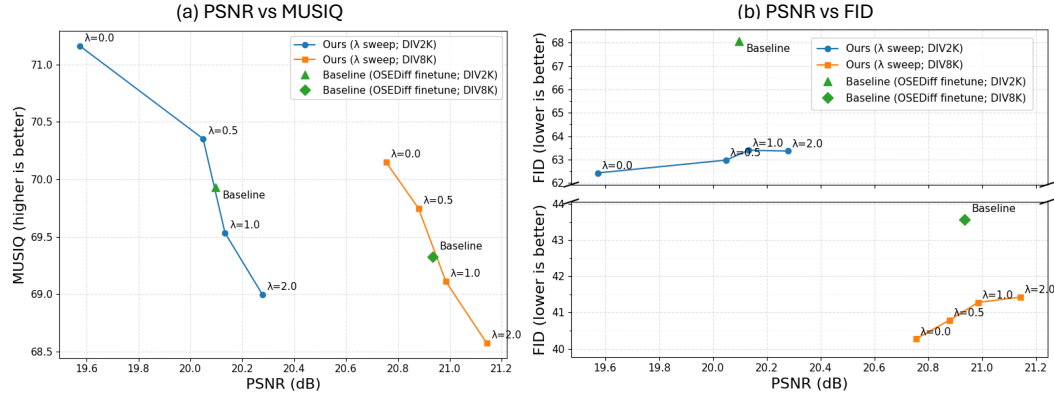


Figure 7: **Trade-off induced by λ_{blur} .** (a,b) PSNR-MUSIQ, PSNR-FID curve. Perceptual quality decreases as λ_{blur} increases.

B ADDITIONAL QUALITATIVE COMPARISON RESULTS

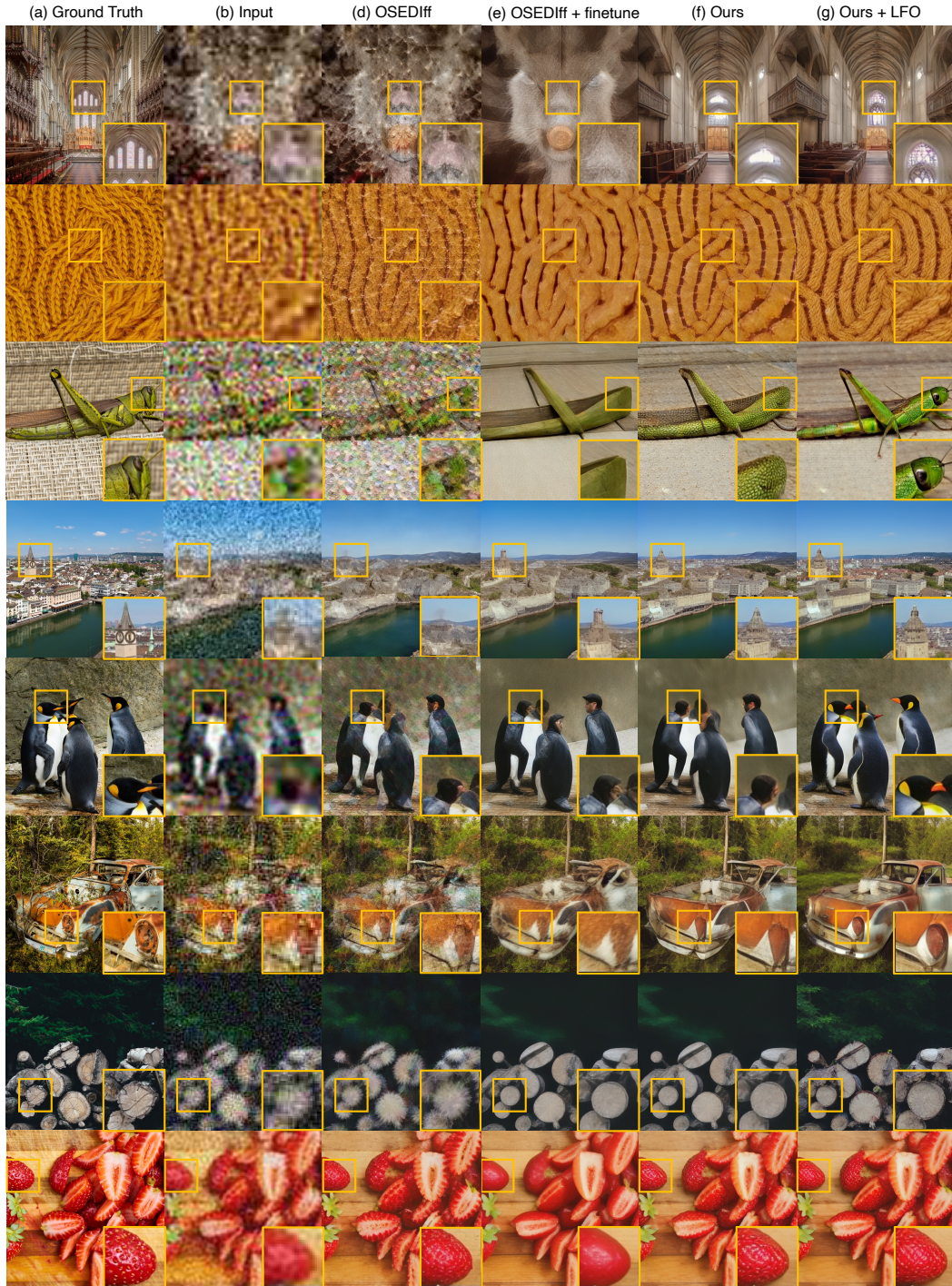


Figure 8: Qualitative Comparison Results.

C ADDITIONAL QUALITATIVE RESULTS OF LQ REFINEMENT WITH RECURSIVE LFO

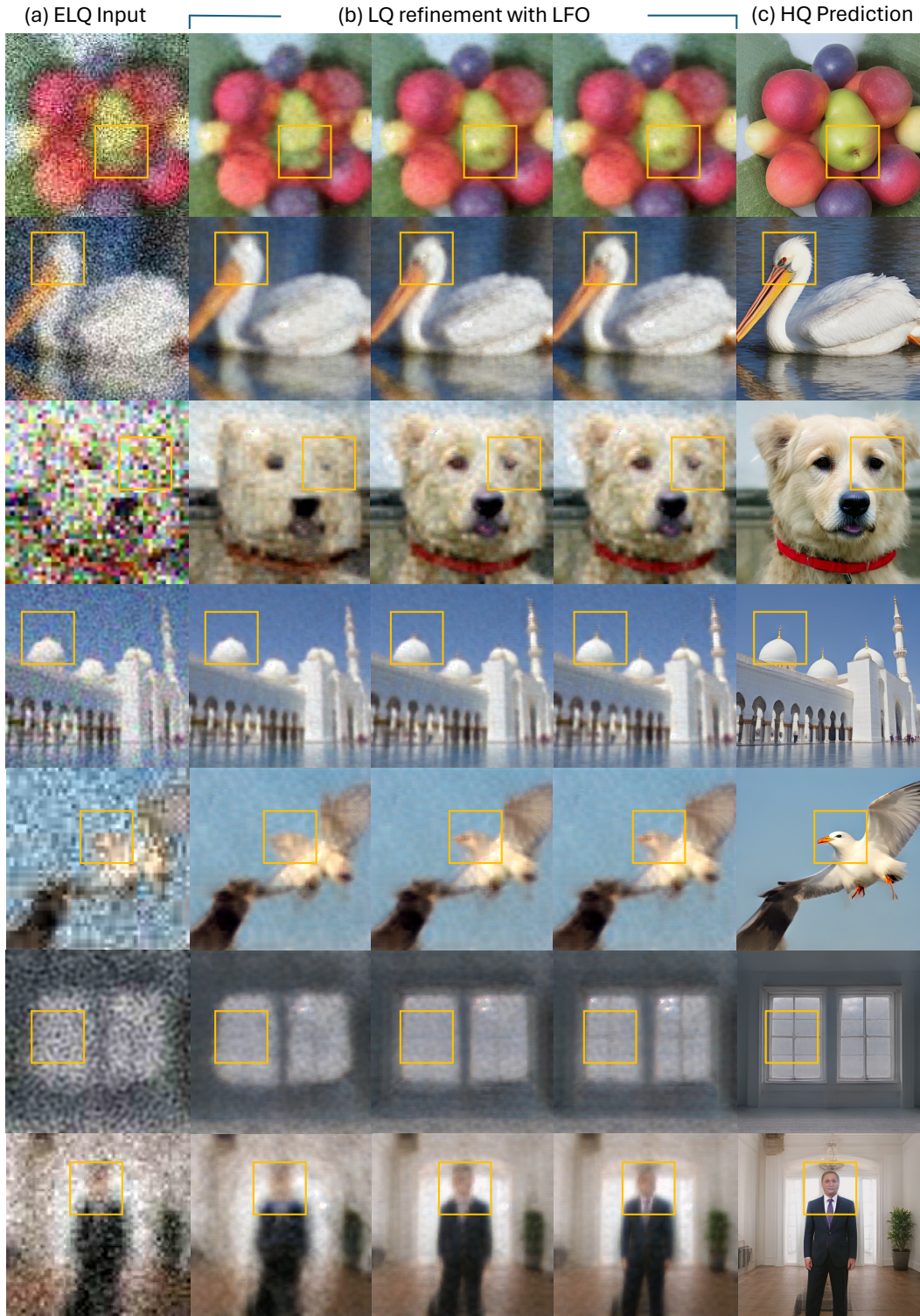


Figure 9: **Qualitative Results of LQ Refinement with Recursive LFO.**

D ADDITIONAL QUALITATIVE RESULTS OF PLUG-AND-PLAY WITH SEESR

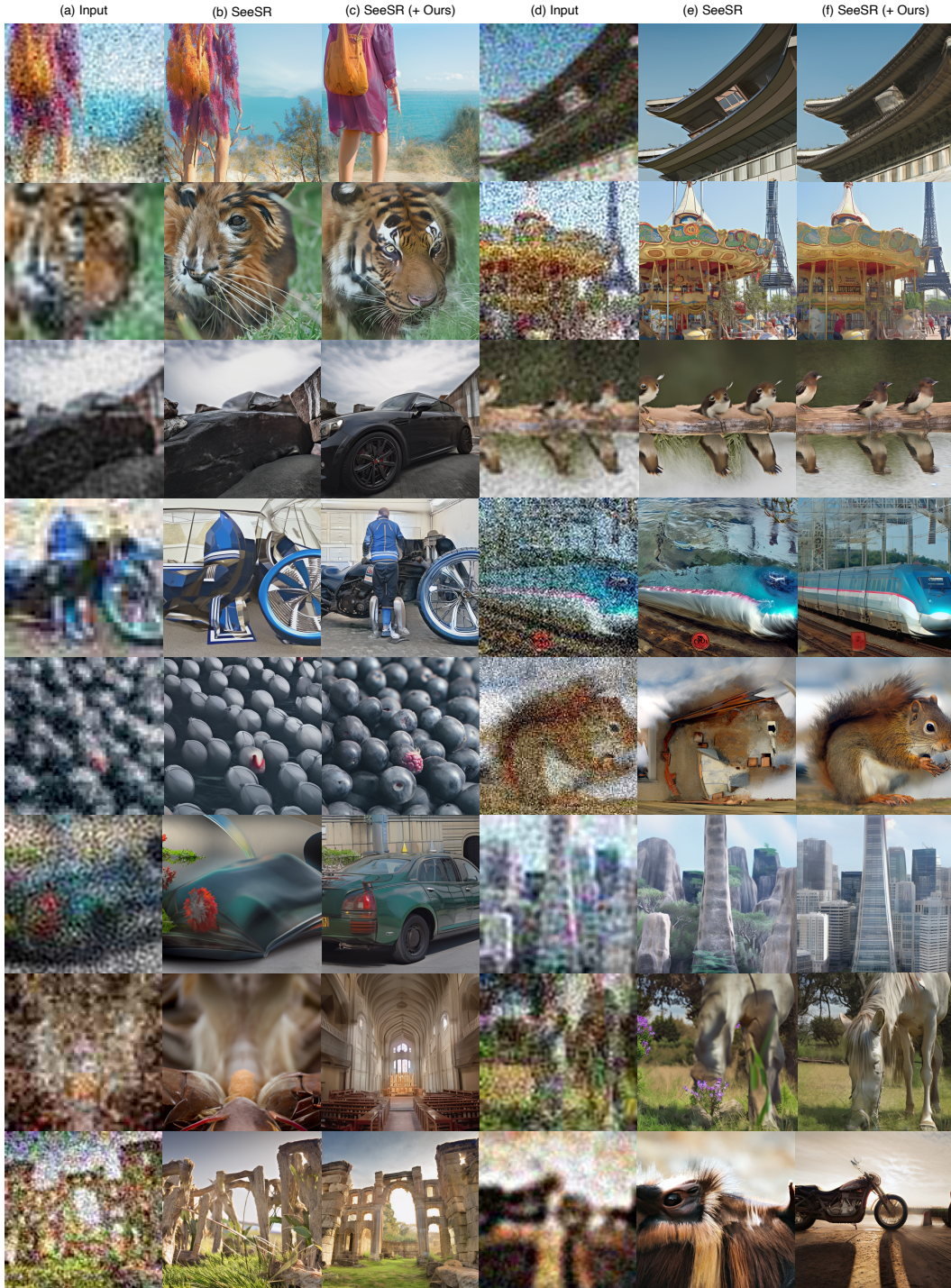


Figure 10: **Qualitative Results of Plug-and-Play with SeeSR.**

E ADDITIONAL QUALITATIVE RESULTS OF PLUG-AND-PLAY WITH S3DIFF



Figure 11: Qualitative Results of Plug-and-Play with S3Diff.

F THE USE OF LARGE LANGUAGE MODELS (LLMs)

LLMs were not involved in research ideation or methodological design and were only used for the purpose of minor expression refinement. The authors retain full responsibility for all scientific content.